BIAXIAL CREEP OF TEXTURED Zr-Nb ALLOYS

Micah Tillman[1], Pratik Joshi[1], Nilesh Kumar[2], Mahmut Cinbiz[3], Korukonda Murty[1]

[1]Department of Nuclear Engineering, North Carolina State University, Raleigh, USA

[2]Department of Material Science and Engineering, University of Alabama, Tuscaloosa, USA

[3]Oak Ridge National Laboratory, P.O. Box 2008, Oak Ridge, TN 37831-6156, USA

Correspondence e-mail: mgtillma@ncsu.edu

The biaxial creep behavior of Nb-added zirconium base alloys—HANA-4 and ZIRLO®—was investigated at 400 and 500°C, respectively. Biaxial creep tests were performed using internally pressurized tubing superimposed with axial load. Both axial and hoop strains were monitored using a linear variable linear variable displacement transducer (LVDT) and a laser telemetric extensometer, respectively. The creep data are analyzed to derive the anisotropy parameters and construct thermal creep loci at a given energy dissipation. The creep locus for HANA-4 was noted to be close to that predicted for isotropy and was found to be not largely affected by initial state. However, the creep locus and anisotropic parameters for cold-worked ZIRLO® showed deviation from isotropy, exhibiting higher hoop deformation compared to axial strain.

I. INTRODUCTION

During light-water reactor operation, zirconium alloy nuclear fuel cladding tubes experience various degradation processes such as water-side corrosion, subsequent hydrogenation of the cladding, and fuel pellet cladding interaction under neutron irradiation at high operating temperatures (325–375°C). Compared to its Zircaloy variants, zirconium's resistance to environmental effects, as well the resistance to radiation damage, is improved by the addition of niobium (Nb) in modern zirconium alloys [1–3].

The thin-walled zirconium alloy cladding tubes are also under a biaxial tensile stress state due to the internal pressure from the fill gases and the gaseous fission products, along with axial forces from radiation growth and end caps. Therefore, the mechanical integrity of the thin-walled cladding tubes must be preserved for safe, reliable operation of nuclear power reactors. Because the cladding is under biaxial loading conditions at elevated temperatures, investigation of the thermal creep deformation of modern and potential future cladding alloys is essential for the prediction of the cladding life [4] and development of high-fidelity nuclear fuel performance codes.

Biaxial thermal creep behavior of zirconium alloy tubes can be understood by analyzing the creep loci [5–8] which reveal effects of grain microstructure, crystallographic texture, and the anisotropy of zirconium alloys [7–9]. This study investigated the biaxial thermal creep behavior of two different Nb-modified zirconium alloys of cold-worked stress-relieved (CWSR) HANA-4 and ZIRLO®. The results are analyzed by the creep loci and compared with earlier work on recrystallized HANA-4 and CWSR Zircaloy-4, respectively.

II. MATERIALS AND METHODS

HANA-4 and ZIRLO® alloy tubing was received from Korea Atomic Energy Institute and Oak Ridge National Laboratory, respectively, and had an average outer diameter of the tubes of 9.43 and 9.53 mm respectively and a thickness of 0.60 mm. Table 1 shows the chemical compositions of both HANA-4 and ZIRLO®. The major differences between these two alloys are in the chromium and tin concentrations. Both of these alloys were received in CWSR condition.

TABLE 1. Nominal compositions [wt %] of HANA-4 and ZIRLO® (Zr is the balance).

Alloy	Nb	Sn	Fe	Cr
HANA-4	1.45	0.41	0.22	0.10
ZIRLO®	1.00	1.00	0.10	-

Biaxial creep

Biaxial creep experiments were performed on an ATS model-2330 lever arm (20:1) creep test machine as shown in Figure 1, with the tube situated in the center of an ATS 3-zone furnace. HANA-4 and ZIRLO® tubes were tested at 500 and 400 °C, respectively. These temperatures were selected based on earlier work on recrystallized HANA-4 and Zircaloy-4. Biaxial stress states were applied to the tubes by internal pressurization superimposed by axial load. The tubes were pressurized with argon gas via a gas booster and air compressor system, and all tests were carried out in air. Temperature was recorded using a K-type thermocouple with an accuracy of ±3°C. The diametral expansion (D_i-D_o) was measured

in-situ with a non-contact laser telemetric extensometer, while the axial elongation was monitored using a linear variable displacement transducer (LVDT).

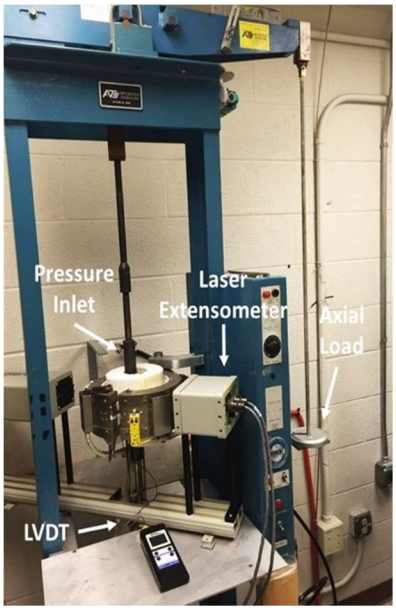

Figure 1. Biaxial creep experimental setup

The tests were performed at multiple stress ratios: α (=σ_θ/σ_z), where σ_θ and σ_z are the hoop and axial stresses, respectively, and σ_r is considered negligible based on thin-wall assumption (diameter/thickness > 10). The following expressions were used to calculate the hoop and axial stresses experienced by the tubing:

$$\sigma_\theta = \frac{PD_i}{2t}, \text{and} \quad (1a)$$

$$\sigma_z = \frac{\sigma_\theta}{2} + \frac{4w}{\pi(D_o^2 - D_i^2)}, \quad (1b)$$

where D_i is inner diameter, D_o is outer diameter, t is the thickness of the tube, w is the applied axial load, and P is the applied internal pressure.

Sample preparation for microstructure

Microstructural examinations for HANA-4 and ZIRLO® were first performed on as-received specimens. The grains were subjected to a focused ion beam (FIB) in a scanning electron microscope (SEM). Since each grain has a different orientation relative to the other, the etching rate was different for each grain. The contrast generated due to this made it possible to examine the grains under SEM. Imaging quality specimens for electron backscatter diffraction (EBSD) were prepared by cutting pieces from the tubes and mechanically polishing them with very fine grit grade pads so that they were thin and flat. Later, the samples were electrochemically polished using the twin-jet method in a solution of 95% methanol and 5% perchloric acid cooled to -60°C at 25V and 10mA for 30s.

III. RESULTS AND DISCUSSIONS

Microstructure

Figure 2 depicts the grain microstructures of HANA-4 and Zirlo in a plane perpendicular to hoop direction, which shows that the grains are elongated along the axial direction. This is expected since the tubes are in cold-worked condition. Figure 3 includes EBSD micrographs which depict the preferred orientations or texture, with predominant basal poles close to normal direction.

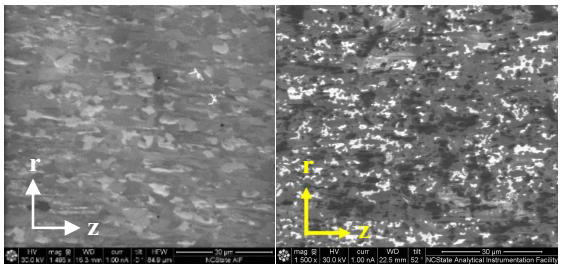

Figure 2. Microstructure imaging along plane normal to hoop direction for HANA-4 (left) and ZIRLO® (right)

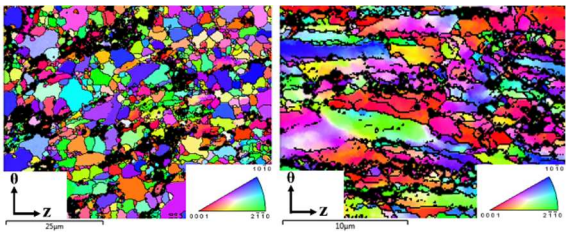

Figure 3: EBSD micrograph of as-received HANA-4 (left) and ZIRLO® (right)

Biaxial creep results

Creep experiments were performed until primary creep transitioned into steady-state creep. Creep curves were formed by plotting the experimental data of deformation as a function of time for each stress at different stress ratios, α (= 0 - 2). Strain rates were obtained from linear fitting of the steady-state creep regions. Figures 4a and 4b include uniaxial creep deformation characteristics of HANA-4 and ZIRLO®. As expected, the steady-state creep rate increases as applied stress is increased. The hoop creep strains were too small to note and thus were not included.

Both hoop and axial creep curves for equi-biaxial loading ($\sigma_\theta=\sigma_z$) are included in Figures 5a and 5b for the two alloy tubes for various stress levels. As for uniaxial tests, the stress levels are changed after attaining steady-states on a single specimen so that sample-to-sample variations are minimized. It is interesting to note that while axial strains are higher than hoop strains for HANA-4 alloy, they are reversed for ZIRLO®, revealing the distinct anisotropy differences between these two alloys.

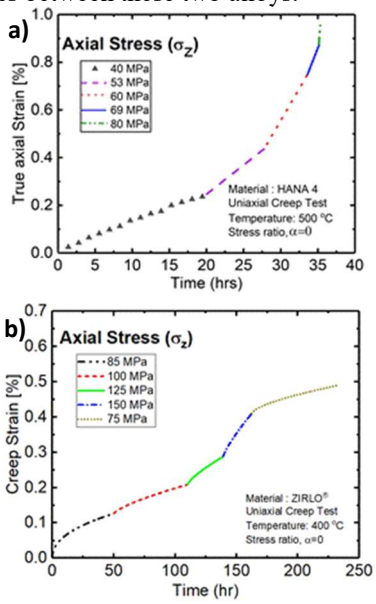

Figure 4. Creep curves from uniaxial creep tests of (a) CWSR HANA-4 at 500°C and (b) CWSR ZIRLO® at 400°C

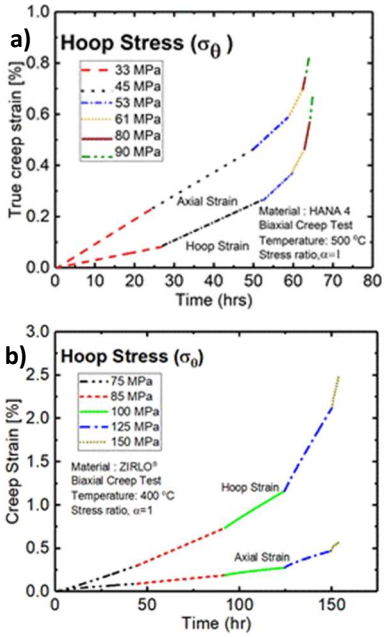

Figure 5. Creep curves from equi-biaxial creep tests of (a) CWSR HANA-4 at 500°C and (b) CWSR ZIRLO® at 400°C

Figures 6a and 6b depict the creep curves for stress ratio α=2: only internal pressurization with no axial load. The axial strains were negligible, so only hoop strains are considered in the analyses. Similarly, such creep curves were obtained at other stress ratios—α = 0.25, 0.5 and 1.5—from which the steady-state strain-rate ratios along hoop and axial directions are noted.

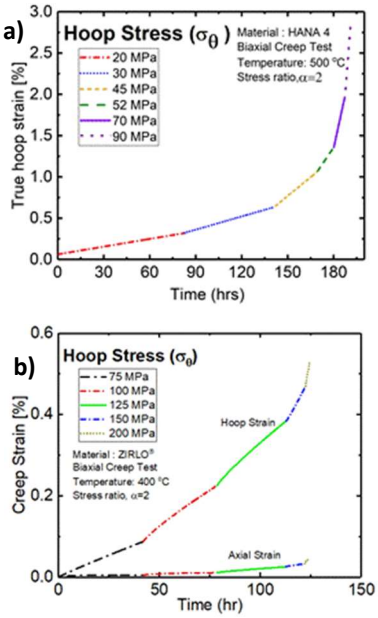

Figure 6. Creep curves from biaxial creep test at stress ratio of 2 of (a) HANA-4 at 500°C and (b) ZIRLO® at 400°C at stress ratio of 2

From the strain rates, work dissipation can be found from the following relationship:

$$\dot{w} = \sum \sigma_i \dot{\varepsilon}_i = \sigma_z \dot{\varepsilon}_z + \sigma_\theta \dot{\varepsilon}_\theta. \qquad (2)$$

where $\dot{\varepsilon}_z$ and $\dot{\varepsilon}_\theta$ are axial and hoop strain rates. The work dissipation rate is obtained for each stress ratio at all stress levels, and Figures 7a and 7b depict the effect of axial stress for HANA-4 and ZIRLO®, respectively. A linear relationship is evident on a double-log plot for both alloys, while a change in slope at lower stresses for HANA-4 reveals a transition expected at lower stresses and/or higher temperatures, as noted by Kombaiah and Murty [10] in Rx-HANA-4. The slopes of these curves correspond to n+1, where n is the stress exponent relating the steady-state strain-rate to stress.

Anisotropy parameters

Hill's equation for anisotropic material is given as follows:

$$F(\sigma_y-\sigma_z)^2+G(\sigma_z-\sigma_x)^2+H(\sigma_x-\sigma_y)^2 +2L\tau_{yz}^2+2M\tau_{zx}^2+2N\tau_{xy}^2=1, \quad (3)$$

where F, G, and H are functions of material yield strengths, and σ_r, σ_θ, and σ_z are principal stresses along normal, transverse, and rolling directions, respectively. This is also the generalized form of Von-Mises criterion for anisotropic materials which is modified by defining

$$R=\frac{F}{H} \text{ and } P=\frac{F}{G}. \quad (4)$$

A generalized stress is defined as the uniaxial yield stress along the rolling direction, which is as follows:

$$\sigma_g^2=\frac{R(\sigma_r-\sigma_\theta)^2+RP(\sigma_\theta-\sigma_z)^2+P(\sigma_z-\sigma_r)^2}{P(R+1)}. \quad (5)$$

For a thin tube with σ_r=0, generalized stress is

$$\sigma_g=\left(\frac{R\alpha^2+(\alpha-1)^2RP+P}{P(R+1)}\right)^{1/2}\sigma_z. \quad (6)$$

The degree of anisotropy can be quantitatively described as R and P parameters, which are defined as:

$$R=\left(\frac{\Delta\varepsilon_\theta}{\Delta\varepsilon_r}\right)_{\varepsilon_z}, \sigma_\theta=\sigma_r=0, \text{and} \quad (7)$$

$$P=\left(\frac{\Delta\varepsilon_z}{\Delta\varepsilon_r}\right)_{\varepsilon_\theta}, \sigma_z=\sigma_r=0, \quad (8)$$

where $\Delta\varepsilon$ is the steady state strain (creep) rate for hoop, axial, and radial directions. Thus, these R and P values are nothing but the transverse contractile strain-rate ratios under uniaxial loading along axial and hoop directions, respectively.

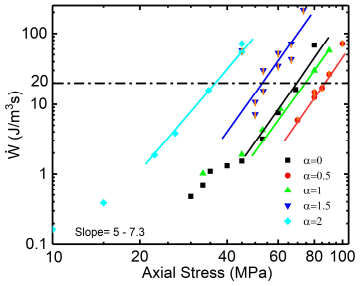

Figure 7a. Work dissipation rate at various stress ratios for HANA-4

It is interesting to note the effect of stress ratio (α) on the ratio of hoop to radial strain-rate ratio (β) that will give R and P values directly. Equations (9a) and (9b) show the relationships, and Figures 8a and 8b are such plots for HANA-4 and Zirlo® alloys, respectively. Since axial strains are negligible in uniaxial axial loading (α=0), R is found from Eq. (10) [9] rather than from Eq. (9a), while P is derived from Eq. (9b):

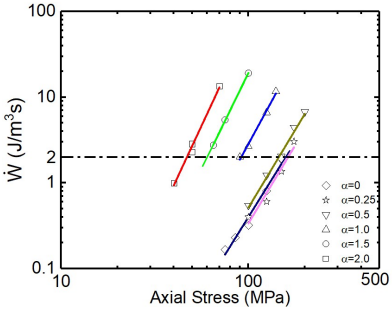

Figure 7b. Work dissipation rate at various stress ratios for ZIRLO®

$$\rho=\frac{\dot\varepsilon_\theta}{\dot\varepsilon_r}=\frac{RP(1-\alpha)-R\alpha}{R\alpha+P}=R \quad (9a)$$

for uniaxial loading (α=0).

$$P=\frac{\alpha}{1-\alpha} \quad \text{for } \rho=0 \quad (9b)$$

$$R=\cot^2\bar\phi \quad (10)$$

where angle $\bar\phi$ represents average peak basal pole angle in the transverse (ND-TD) plane.

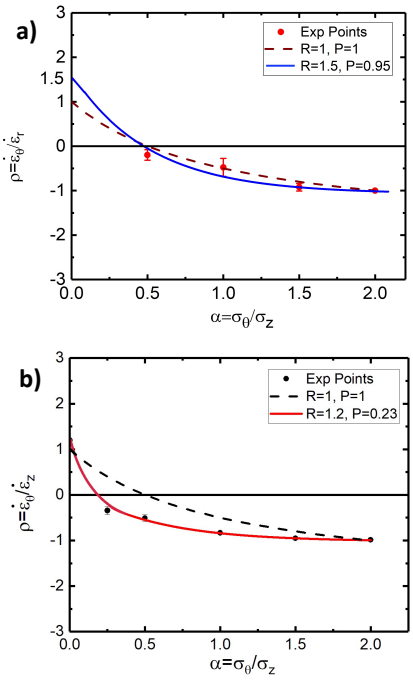

Figure 8. ρ versus α for (a) CWSR HANA-4 at 500°C and (b) CWSR ZIRLO® at 400°C

The values for R and P are thus found to be as follows.

R=1.50 and P=0.95 for HANA-4 (11a)
R=1.20 and P=0.26 for ZIRLO® (11b)

These values compare with those found earlier for recrystallized HANA-4 (1.25 and 1.08) [10] and CWSR Zircaloy-4 (1.25 and 0.30) [9], respectively.

Creep Loci

While yield loci are defined at the yielding of the materials, such loci for creep must have a criterion since creep can take place at any loading condition. Adams and Murty [8] suggest considering hoop and axial stresses at a specified dissipation rate, and thus the constant rates of 20 J/m^{3}s and 2 J/m^{3}s were used for HANA-4 and ZIRLO®, respectively. Creep loci of both alloys were plotted by taking a constant work dissipation-rate on the log-log graphs of work dissipation rate vs. axial stress (Figures 7a and 7b), leading to axial versus hoop stresses. The constant rates used for HANA-4 and ZIRLO® were 20 J/m^{3}s and 2 J/m^{3}s respectively, as these values were found to lie in the power-law creep region. The intersection of the slopes for each stress ratio provides the axial stress, and the corresponding hoop stress is calculated by the associated stress ratio. Figure 9 shows the creep loci for ZIRLO® and HANA-4 plotted as normalized stresses, along with that for isotropy (R=P=1) as reference. HANA-4 creep locus is close to isotropy, which is not the case for ZIRLO®, which exhibited R&P values of 1.2 and 0.26 respectively.

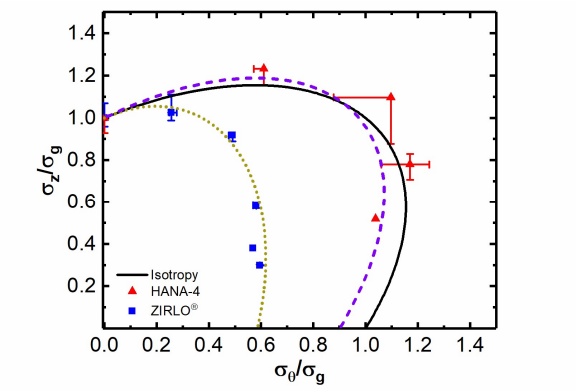

Figure 9. Creep loci for HANA-4 and ZIRLO® compared with that for isotropy

IV. SUMMARY AND CONCLUSIONS

Biaxial creep tests were successfully conducted on Nb-added Zircaloys in as-received condition at stress ratios from 0 to 2 and various stress levels. The creep locus for HANA-4 is close to isotropy, with essentially no effect on initial condition. On the other hand, ZIRLO® exhibited stronger creep anisotropy, with relatively weaker hoop direction, as noted earlier in CWSR Zircaloy-4. Work is now underway on the development of crystallite orientation distribution functions (CODF) to combine with slip models to predict the creep loci.

ACKNOWLEDGMENTS

This work is supported by the National Science Foundation grant #CMMI1727237, and we thank Andy Nelson of Oak Ridge National Laboratory for his interest.

REFERENCES

[1] G.P. Sabol, ZIRLO an Alloy Development Success, in: 14th ASTM Int. Symp. Zr Nucl. Ind., Stockholm, 2005: pp. 3–24.
[2] M. Steinbrück, M. Böttcher, Air oxidation of Zircaloy-4, M5® and ZIRLO™ cladding alloys at high temperatures, J. Nucl. Mater. 414 (2011) 276–285.
[3] A. Couet, A.T. Motta, R.J. Comstock, Hydrogen pickup measurements in zirconium alloys: Relation to oxidation kinetics, J. Nucl. Mater. 451 (2014)1–13.
[4] K.L. Murty, Creep studies for Zircaloy life prediction in water reactors, J. Mater. Miner. Met. 51 (1999) 32–39.
[5] H. Stehle, E. Steinberg, E. Tenckhoff, Mechanical properties, anisotropy, and microstructure of Zircaloy canning tubes, in: Zircon. Nucl. Ind. ASTM STP 633, American Society for Testing and Materials, 1977: pp. 486–507.
[6] J. Schroeder, M.J. Holicky, On secondary creep of anisotropic nuclear materials, J. Nucl. Mater. 33 (1969) 52–63.
[7] J.C. Earthman, K.L. Murty, B. V Tanikella, J.C. Britt, Effects of grain-shape anisotropy and texture on balanced-biaxial creep of Ti and Zr alloys, J. Mater. Miner. Met. October 19 (1994) 48–54.
[8] B. L. Adams and K.L. Murty "Biaxial Creep of Textured Zircaloy: Part II - Crystal-Mean Plastic Modeling," Mat. Sci. Eng., 70, 181–190 (1985).
[9] K. Linga Murty, I. Charit, Texture development and anisotropic deformation of zircaloys, Prog. Nucl. Energy. 48 (2006) 325–359.
[10] Nilesh Kumar, Kailtin Grundy, Boopathy Kombaiah, Baifeng Luan and K. L. Murty, "Anisotropic Biaxial Creep of Textured Nb-modified Zircaloy-4 Tubing," in Proceedings of

the SMD symposium honoring Prof. K. Linga Murty on “Mechanical and Creep Behavior of Advanced Materials,” TMS, 2017, pp. 19–32.